Atomically Thin Delta-Doping of Self-Assembled Molecular Monolayers by Flash Lamp Annealing for Si-Based Deep UV Photodiodes

Chang, S.; He, J.; Prucnal, S.; Zhang, J.; Zhang, J.; Zhou, S.; Helm, M.; Dan, Y.;

Originally published:

June 2022

ACS Applied Materials and Interfaces 14(2022)26, 30000-30006

DOI: https://doi.org/10.1021/acsami.2c04002

Atomically Thin Delta-Doping of Self-Assembled Molecular Monolayers by Flash Lamp Annealing for Si-Based Deep UV Photodiodes

Shannan Chang[1,2], Jiajing He[1,2], Slawomir Prucnal[3], Jieyin Zhang[4], Jianjun Zhang[4], Shengqiang Zhou[3], Manfred Helm[3], Yaping Dan[1,2*].

[1]National Key Laboratory of Science and Technology on Micro/Nano Fabrication, Shanghai Jiao Tong university, Shanghai, 200240, China

[2]University of Michigan – Shanghai Jiao Tong University Joint Institute, Shanghai Jiao Tong university, Shanghai, 200240, China

[3]Helmholtz-Zentrum Dresden-Rossendorf, Institute of Ion Beam Physics and Materials Research, Bautzner Landstrasse 400, D-01328 Dresden, German

[4]National Laboratory for Condensed Matter Physics and Institute of Physics, Chinese Academy of Science, 100190 Beijing, China

[*] To whom correspondence should be addressed. Email: yaping.dan@sjtu.edu.cn

Abstract

Delta doping (δ-doping) can find a wide range of applications in advanced metal oxide semiconductor field effect transistors, deep UV photodetectors, quantum devices, and others. In this work, we formed a δ-doping layer in silicon by employing flash lamp annealing to treat the PCl_3 monolayers grafted on silicon surfaces. The δ-doping layer is atomically thin (<1 nm). Low-temperature Hall measurements show that the δ-doping layer is in a metallic state and exhibits a weak localization phenomenon, implying that a two-dimensional electron gas is formed. When we form such an n-type δ-doping layer on a highly doped p-type Si substrate, a highly sensitive solar-blind UV photodetector is created, which traditionally was only possible by using wide band gap semiconductors such as gallium nitride (GaN) or silicon carbide (SiC).

Introduction

Delta-doping (δ-doping) can find a wide range of applications in quantum devices, (1) deep UV photodetectors, (2) complementary metal oxide semiconductor (CMOS) field effect transistors, (3,4) and so forth. (5−7) Deep UV photodetectors are taken as an example. Traditional silicon-based photodiodes are not sensitive in the deep UV spectrum, although deep UV photons can be absorbed by silicon. This is because commercial photodiodes are made of a vertical structure with the surface being highly doped to suppress the leakage of current through surface states. The thickness of the doping surfaces is often in the range of tens of nanometers to submicrometers formed by ion implantation or thermal diffusion. In contrast, the penetration depth of photons dramatically drops from the micrometer scale in the visible spectral range to sub-10 nm in the deep UV spectrum. As a result, photons in the deep UV spectrum are all absorbed in the highly doped surface layer which is electrically neutral. Electron–hole pairs generated by the deep UV spectral absorption will not be efficiently separated and collected as a photocurrent, resulting in extremely weak photoresponsivity. (8)

In this work, we demonstrate a δ-doping technology by treating a self-assembled phosphorus trichloride (PCl_3) monolayer on silicon surfaces with a flash lamp annealing (FLA) process. (9,10) The δ-doping is atomically thin and forms a two-dimensional (2D) electron gas in silicon in which electrons exhibit weak localization. A Si-based pn junction photodiode was fabricated by forming an n-type δ-doping layer on a p-type Si substrate. The atomically thin metallic δ-doping layer formed by the FLA process allows photons in the deep UV spectral range to be absorbed in the depletion region of the diode, as a result of which the Si-based device becomes highly sensitive in the deep UV spectral range.

Results and Discussion

Figure 1 shows the δ-doping process using phosphorus precursors on a silicon-on-insulator (SOI) substrate by FLA. The device layer is intrinsic with a resistivity of 10 kΩ·cm and was patterned into 2 mm × 2 mm squares. The four corners of the sample were first implanted with phosphorus with a concentration of $\sim 10^{19}$ cm^{-2} for better metal contacts, followed by rapid thermal annealing (RTA) at 1000 °C for 30 s to activate the dopants. Whereafter, Si samples were cleaned and immersed in a 0.5% solution of hydrofluoric acid (HF) for a short time (5 s) to form surfaces terminated with S–OH (possibly mixed with Si–H). To form self-assembled dopant monolayers, the samples were kept in the mixture of PCl_3, triethylamine, and benzene solution at 70 °C for 24 h. PCl_3 was used as the phosphorus dopant carrier to minimize possible carbon contaminations. (11,12) Afterward, the samples were sonicated sequentially in CMOS grade acetone, ethanol, and deionized (DI) water for 3 min each to remove the residual chemicals of physical absorption. Some of the samples were taken for surface analysis, and the rest went through the processes for FLA, which will be described later.

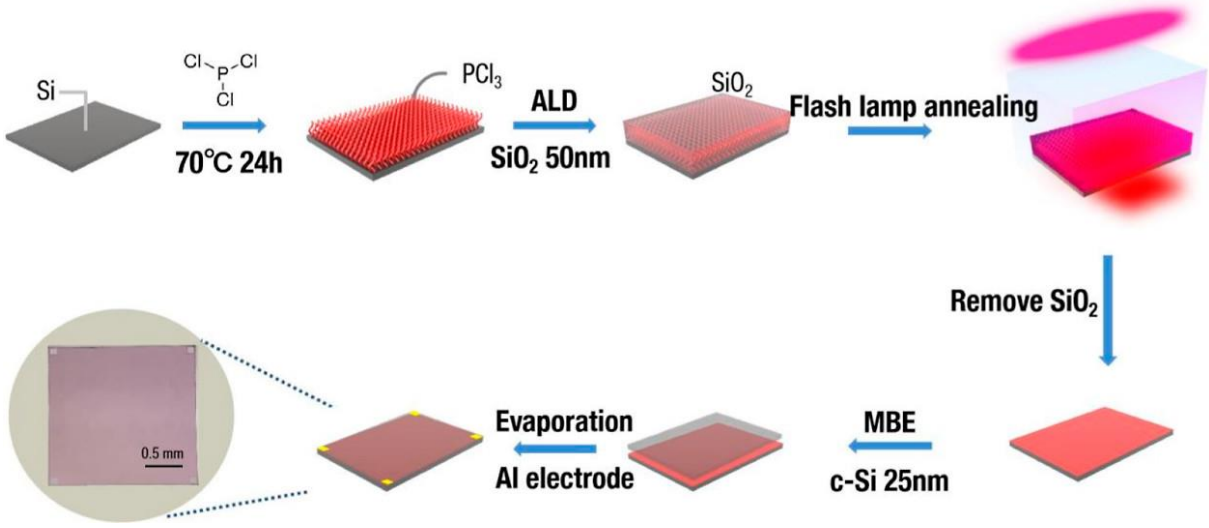

Figure 1. Schematic of the δ-doping process using phosphorus precursors and FLA.

X-ray photoelectron spectroscopy (XPS) was performed for the blank sample and the surface-functionalized sample as shown in Figure 2. Clearly, there is only a broad Si plasma loss peak for the blank sample in Figure 2a. In contrast, for the surface-functionalized sample, the broad Si 2s plasmon loss peak has a side shoulder located at approximately 191.4 eV which is attributed to the P 2s peak (Figure 2b). (13) This indicates that PCl_3 has been successfully grafted on the silicon surface. The binding energy of Cl 2s in the XPS spectrum is known to be 270 eV. (14) However, our XPS spectrum shows no signal near this energy range, as shown in Figure 2c. Therefore, it is most likely that the reaction given in eq 1 occurs during the PCl_3 self-assembly process. (12) In this process, each phosphorus atom binds

to three silicon atoms via oxygen atoms as shown in the inset of Figure 2c, while the Cl elements are removed in the form of HCl.

$$PCl_3 + 3Si - OH \rightarrow P(O - Si)_3 + 3HCl \quad (1)$$

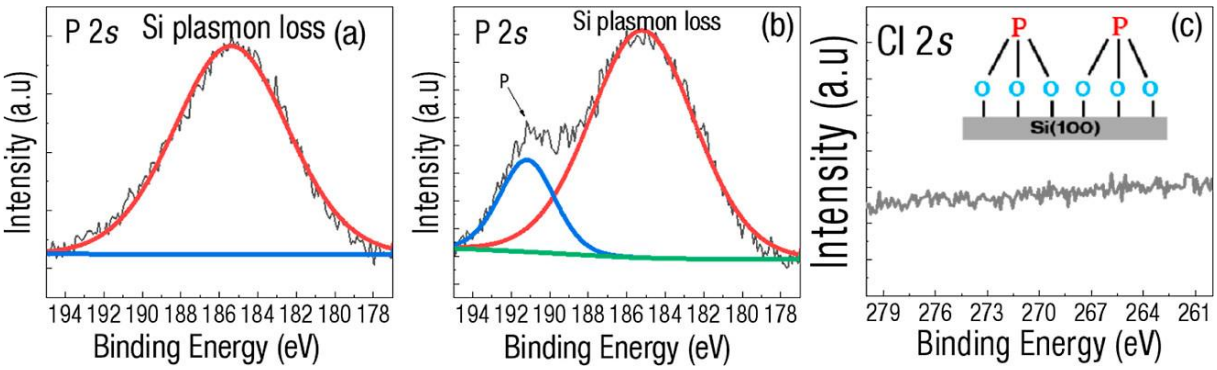

Figure 2. XPS narrow scans of P 2s for (a) blank sample and (b) phosphorus-functionalized sample. (c) XPS narrow scan of Cl 2s for the same sample as (b). Inset: chemical structure of Si–O–P.

For the samples that were to be treated with FLA, a layer of 50 nm thick SiO_2 was deposited on the sample surfaces by atomic layer deposition (ALD) after PCl_3 grafting. The samples were then placed in a FLA chamber with a continuous N_2 flow. To minimize the thermal stress, the halogen lamps were used to preheat the sample to an intermediate temperature before reaching the peak temperature by subsecond flash. Details of FLA can be found in ref (10). We kept the maximum energy density at 149.3 J/cm^2, and the preheated temperature for FLA was varied in the range from 400 to 500 K. The pulse length of the flash was fixed at 3 or 20 ms.

Right after FLA, the SiO_2 protective layer was removed in HF followed by a 25 nm thick crystalline Si growth by molecular beam epitaxy (MBE). A distinct crystalline interface can be observed at the atomic scale using high-resolution transmission electron microscopy (HRTEM) as shown in Supporting Information, Figure S1. The growth of crystalline Si prevents the Si–H dimer contamination in phosphorus profiling (see the related discussion later). Al electrodes were deposited on the sample to make electrical contacts on the four predoped corners (see the Materials and Methods section for details). The sheet resistances of the samples were obtained from van der Pauw measurements. Figure 3a shows the dependence of sheet resistance on various FLA parameters. The sheet resistance drops dramatically from ~17.3 to 1.6 kΩ/sq as the energy density deposited on the sample surface by FLA increases. The decrease in sheet resistance means more dopants have diffused into the silicon lattice and are electrically activated. The nonmolten silicon surface remains atomically flat when the samples are treated with an energy density of 149.3 J/cm^2 for 20 ms with a preheat temperature of 450 °C or lower for 30 s. At a higher preheat temperature, the sample surface became molten, (15) which causes the surface roughening as shown in the inset of Figure 3a.

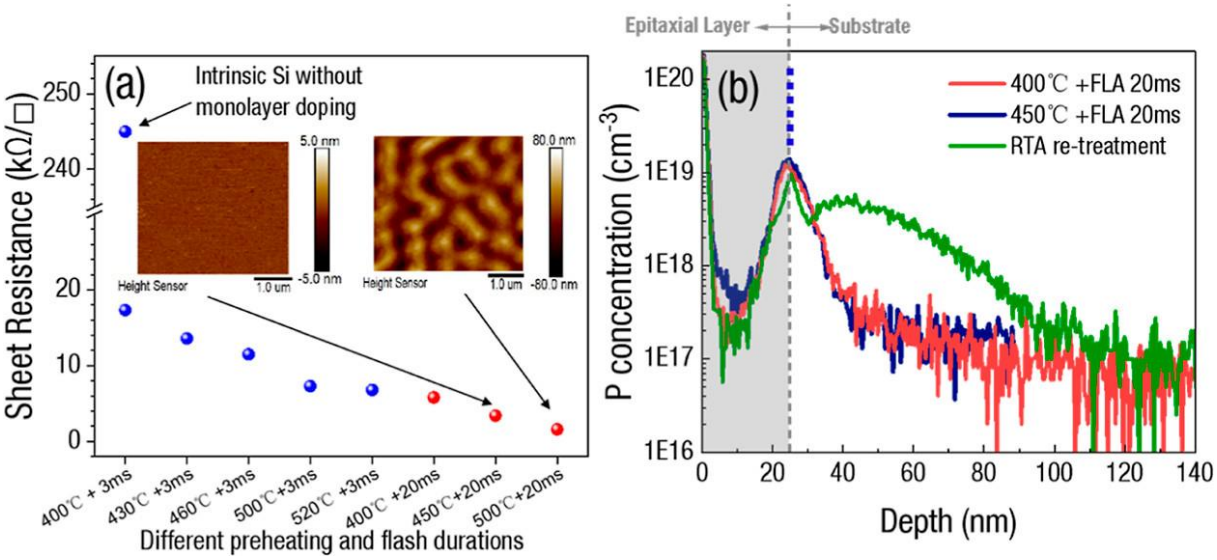

Figure 3. (a) Sheet resistances of the P-functionalized SOI substrate at various preheating temperatures and FLA durations with a flash energy density of 149.3 J/cm^2 (insets are the atomic force microscopy images of the sample surfaces). (b) SIMS depth profiles for the samples S1 (red), S2 (blue), and S2 with an additional RTA treatment (green). The dashed blue line represents δ-doping.

To probe the dopant profile after the FLA treatment (samples S1 and S2), we employed secondary ion mass spectrometry (SIMS). Samples S1 and S2 were annealed using 400 °C + FLA 20 ms and 450 °C + FLA 20 ms, respectively. Among all nonmelt samples, only these two samples have the lowest sheet resistance, implying that δ-doping is most likely formed in these two samples. Both samples have a comparable dopant profile with a peak concentration of ∼1.3 × 10^{19} cm^{-3} at the epitaxial interface, as shown in Figure 3b. The phosphorus concentration declines rapidly toward both sides at a rate of 8 nm/decade (see Supporting Information, Figure S2). The abrupt increase toward the surface (left side of Figure 3b) is caused by the false signals of Si–H dimers from surfaces that have the same mass as phosphorus. When integrating the dopant concentration along the *x* coordinate (abrupt increase near the surface is excluded), we found that the dopant concentration per unit area is 1.12 × 10^{13} and 1.27 × 10^{13} cm^{-2} for S1 and S2, respectively. Surprisingly, the electron concentration taken from Hall effect measurements for these two samples is 1.28 × 10^{13} and 1.8 × 10^{13} cm^{-2} (see Supporting Information, Figure S3), respectively, higher than the P dopant concentration collected from SIMS in both cases. Previously, Polley et al. showed that a regular SIMS has a limited spatial resolution and therefore cannot resolve the δ-doping formed by MBE. (16) We suspected that a δ-doping layer is also hidden in our samples and cannot be well resolved by SIMS. To ensure that the dopants can be resolved by SIMS, we applied an additional RTA (17) process to treat the sample at 1050 °C for 30 s. After the treatment, the δ-doping layer will spread out, and additional dopants will be detected by SIMS. Indeed, we observed an additional broad bump extended into the bulk (green curve) in the SIMS profile of the sample S2 after the RTA treatment. The integrated P concentration increases from 1.27 × 10^{13} to 2.55 × 10^{13} cm^{-2}. This indicates that the δ-doping at the interface reaches a concentration of ∼1.28 × 10^{13} cm^{-2}.

Since the SIMS system (EAG Laboratories) has a depth resolution of 1 nm, it would be safe to assume that phosphorus atoms in the δ-doping layer are accumulated within 1 nm near the interface of the Si substrate and the epilayer, probably a few atomic layers thick. This assumption will place the δ-doping at the interface at a concentration of 1.28 × 10^{21} cm^{-3} or higher, which is well beyond the solubility of phosphorus in silicon (∼7 × 10^{20} cm^{-3} at 1300 °C). (18,19) Clearly, a supersaturated δ-doping layer is

formed. Next, we estimated the electron concentration that this δ-doping layer contributes to. As we found previously, the total electron concentration of the sample S2 is 1.8×10^{13} cm^{-2}. The phosphorus dopants excluding those in the δ-doping layer were previously profiled by SIMS to be 1.27×10^{13} cm^{-2} (the blue curve in Figure 3b) which contribute to an electron concentration of 1.2×10^{13} cm^{-2} according to the theoretical concentration-dependent ionization of phosphorus (20) (see Supporting Information, Figure S4, for calculation details). This means that the additional electron concentration of 0.6×10^{13} cm^{-2} comes from the δ-doping layer. This value is close to the electron concentration we later found in the metallic state, consistent with the fact that a 2D electron gas is formed in the δ-doping layer.

A 2D electron gas from a δ-doping layer buried inside semiconductors will exhibit quantum effect in carrier transport. (21) For this reason, we characterized the charge carrier transport at low temperature when a tunable magnetic field was applied perpendicular to the sample surface. At zero magnetic field, the sheet resistance of both samples (S1 and S2) monotonically decreases as the temperature decreases to 2 K, as shown in Figure 4a. This indicates that the δ-doping layer is degenerate. The sheet resistance at 2 K will reach 1.33 and 0.93 kΩ/sq for the samples S1 and S2, respectively. Accordingly, Hall effect measurements show that the electron concentration and electron mobility at this temperature are 4.06×10^{12} cm^{-2} and 1158 cm^2/V s and 6.6×10^{12} cm^{-2} and 1017 cm^2/V s for the samples S1 and S2, respectively, as shown in Table 1. The electron concentration in the metallic state of the sample S2 found from the Hall measurements is consistent with what we found above from SIMS profiling before and after the RTA process.

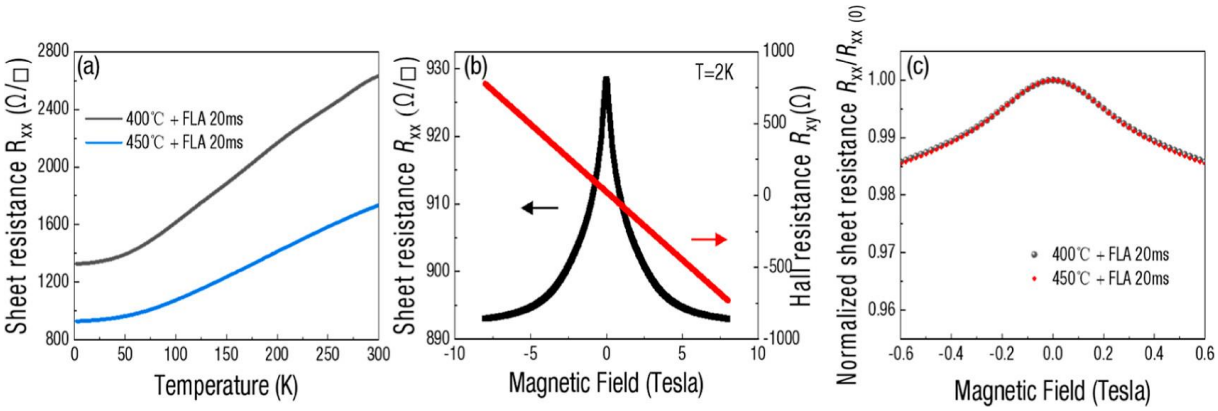

Figure 4. (a) Temperature dependence of the sheet resistances for the samples S1 and S2. (b) Sheet resistances R_{xx} (black line) and Hall resistances R_{xy} (red line) of the sample S2 as a function of magnetic field at T = 2 K. (c) Normalized magnetoresistances dependent on the magnetic field for S1 and S2.

Table 1. Parameters Found from Hall Effect Measurements at 2 K

sample description	**S1 (400 °C + FLA 20 ms)**	**S2 (450 °C + FLA 20 ms)**
N_e (cm^{-2})	4.06×10^{12}	6.61×10^{12}
R_{xx}(0) (Ω/□)	1326	928
μ (cm^2/V s)	1158	1017
B_0 (T)	4.4	18.2

sample description	S1 (400 °C + FLA 20 ms)	S2 (450 °C + FLA 20 ms)
B_ϕ (T)	0.07	0.05
τ_ϕ (ns)	0.1	0.2
l_ϕ (nm)	50	60

Figure 4b shows the magnetoresistance R_{xx} of the S2 sample at 2 K. The resistance decreases monotonically when the applied magnetic field intensity increases in both directions. This phenomenon can be explained with the theory of weak localization. (22) It is known that electrons in semiconductors do not simply follow ballistic transport but experience a series of random scatterings even at low temperature. Due to inelastic scatterings, (23−25) these random scatterings more likely result in some electrons wandering around in a circle, that is, weakly localized, in particular when electrons transport in a 2D plane. Externally applied magnetic fields will break the weak localization of the electrons, as a result of which the electrons will more likely transport in a classical way of elastic scatterings, causing a decrease in resistance (magnetoresistance). The weak localization theory has been well studied. (23,26−29) Previous studies (30) have shown that both spin and spin–orbit scatterings in P-doped silicon are weak. This means that the relaxation times associated with these scatterings are long and can be neglected when compared with the electron–electron and electron–phonon interactions. The decrease in resistance or increase in conductance as a function of applied magnetic field B is given by the simplified Hikami model as shown in eq 2. (28)

$$\frac{\Delta\sigma_{WL}}{\sigma_{WL,0}} = \psi\left(\frac{1}{2}+\frac{B_\varphi}{B}\right) - \psi\left(\frac{1}{2}+\frac{B_0}{B}\right) \quad (2)$$

in which $\Delta\sigma_{WL}$ is the weak localization contribution to the magnetoconductance, $\sigma_{WL,0}$ is the conductance at $B = 0$, and ψ is the digamma function that is the logarithmic derivative of the gamma function. The characteristic fields B_0 and B_ϕ are associated with the transport relaxation mechanisms of impurity potential scatterings and inelastic scatterings, respectively.

We extracted B_0 and B_ϕ in Table 1 by fitting eq 2 to the experimental data in Figure 4c. As known, it is the inelastic scatterings that cause the loss of electron phase coherence and result in the weak localization of electrons. The characteristic magnetic field B_ϕ associated with the inelastic scatterings is our focus here. The electron phase coherence is often characterized with the phase coherence length l_ϕ and phase relaxation time τ_ϕ, which are measures of how long an electron retains its phase information in space and time domains and therefore are important parameters for solid-state qubits in a quantum computer. According to Goh et al., (31) the phase coherence length l_ϕ is correlated with the characteristic magnetic field by $B_\varphi = \frac{\hbar}{4el_\varphi^2}$, which is 50 and 60 nm for S1 and S2, respectively. The phase relaxation time τ_ϕ is dependent on the phase coherent length as $l_\varphi = \sqrt{D\tau_\varphi}$, where D is the diffusion coefficient correlated with the mobility μ by $D = \frac{\mu kT}{q}$, where k is the Boltzmann constant, T is the absolute temperature, and q is the unit of charges. For the samples S1 and S2, the phase relaxation time τ_ϕ is 0.1 and 0.2 ns, respectively.

The above temperature-dependent Hall effect measurements have demonstrated that δ-doping in the metallic state is indeed formed in our monolayer doped Si substrate by FLA. This metallic δ-doping layer can be used to enhance the photoresponsivity in the deep UV spectrum of Si-based photodetectors. Traditional Si photodetectors suffer from low responsivities in the deep UV range (32,33) because most of the UV light is absorbed in a very thin layer right below the Si surfaces, which are often within the highly doped charge-neutral region. Photogenerated electron–hole pairs in this

region cannot be efficiently separated and thus have little contribution to the photocurrent. Our metallic δ-doping layer has reduced the top highly doped n-type Si to the atomic scale, as a result of which the deep UV photoresponsivity will be significant improved. The Si-based UV detector was fabricated on a p^+-type Si substrate (~0.02 Ω·cm) following the steps illustrated in Figure 1 except for the SiO_2 removal and MBE growth. The sample was treated with FLA under the same condition as the sample S2 (450 °C for 30 s + 149.3 J/cm^2 for 20 ms). To ensure that the Al electrodes can make proper contacts with the metallic δ-doping layer, the contact area in the Si wafer (at the corners of a 2 mm × 2 mm Si wafer) was preimplanted with phosphorus ions at a concentration of 10^{19} cm^{-3} as the very first step in Figure 1. The final device structure is depicted in the inset of Figure 5a.

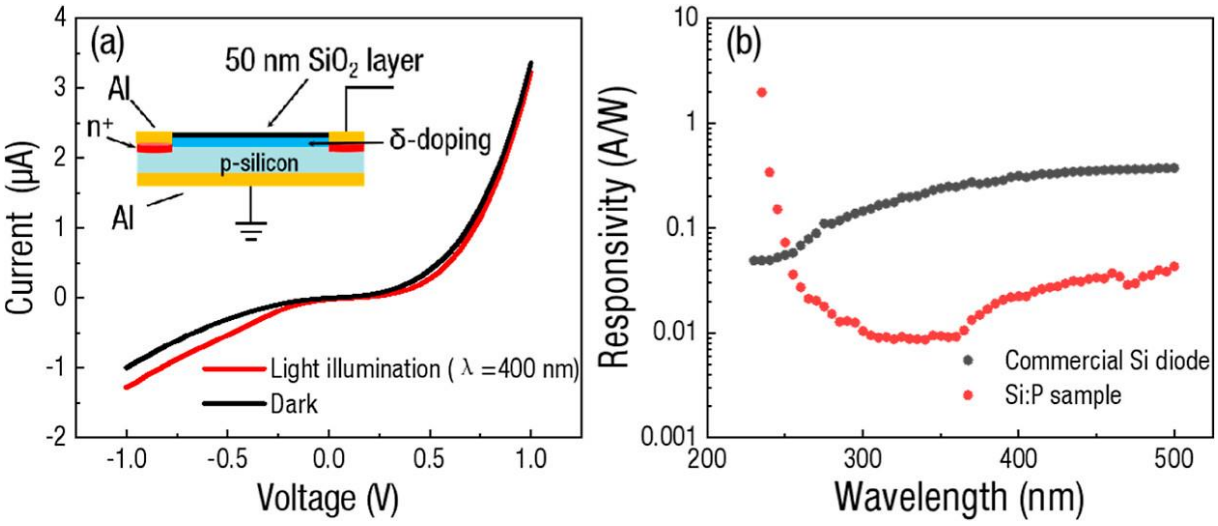

Figure 5. (a) *I–V* curves of the δ-doping photodiode in the dark and under light illumination (λ = 400 nm). Inset: Diagram of the device structure. (b) Spectral photoresponse from 230 to 500 nm of the δ-doping photodiode and a commercial Si pin photodiode. The device is biased at −1 V.

Figure 5a shows the *I–V* curves of a Si diode with a δ-doping layer in the dark and under light illumination. The dark current exhibits a rectifying behavior like a pn junction diode. The depletion region width is ~28 nm by estimation. The leakage current is surprisingly larger than expected at a negative bias probably because the δ-doping layer is not uniform at a large scale, and surface states in the area where δ-doping is not formed will create a shunt resistance for the pn junction diode. The device exhibits a relatively large photocurrent under light illumination (the red line in Figure 5a). The spectral response of the device is shown in Figure 5b (red curve). The photoresponse increases to ~1 A/W when the wavelength decreases to 230 nm. The high photoresponse of our device at short wavelengths is simply because the penetration depth of photons in the deep UV spectral range is reduced to less than 10 nm. Our δ-doping layer allows most of the UV photons to be absorbed in the depletion region of the photodiodes, as a result of which the photo-generated electron–hole pairs can be separated by an electric field as a photocurrent. In contrast, typical photodiodes have a thick highly doped surface layer (tens of nanometers or more in thickness) formed by ion implantation or thermal diffusion. Most of the deep UV photons are absorbed in the highly doped region which is electrically neutral. The photo-generated electron–hole pairs cannot be efficiently separated and contribute to the photocurrent. Indeed, when we calibrated the spectral response of a commercial p–i–n photodiode, the photoresponsivity decreases by 1 order of magnitude from 0.4 to 0.05 A/W when the wavelength is decreased from 500 to 230 nm (the black curve in Figure 5b).

The silicon substrate in our photodiode is highly doped (10^{18} cm^{-3}), which results in a short depletion region (~28 nm) right below the metallic δ-doping layer. Interestingly, this short depletion region significantly reduces the photoresponsivity at longer wavelengths, creating a solar blind photoresponse which is very much needed in practical applications. We also measured the light absorption spectrum and calculated the photoresponsivity of the device by assuming a 100% efficiency of photocarrier separation within the depletion region. Similarly, high responsivities at short wavelengths and low responsivities at long wavelengths were also observed, as shown in Supporting Information, Figure S5. Traditionally, this sort of unique solar-blind UV photodetectors can only be possible by using wide band gap semiconductors. It is now achieved by forming a metallic n-type δ-doping on a highly doped p-type silicon substrate.

Conclusions

In this work, we demonstrated a new δ-doping technique by treating the self-assembled molecular monolayer with FLA for 3 or 20 ms. The dopants were confined in a few atomic layers where a 2D electron gas was formed. We applied this technique to create a pn junction diode by forming a top δ-doping n^+ layer on a p-type silicon wafer, as a result of which the photoresponses of the device in the deep UV spectrum have been significantly enhanced. With this technology, Si-based deep UV imaging technology may be readily realized by leveraging the state-of-the-art CMOS technology.

Materials and Methods

Wafer Preparation

The bare Si wafer was cleaned by standard RCA steps. After soaking in HF solution and subsequently in DI water both for 1 min, the samples were taken out and dried in N_2. A negative photoresist was spin-coated on the sample surfaces. Photolithography was employed to pattern four corners of the samples for P ion implantation. The P dopants at a concentration of 10^{19} cm^{-3} were activated by RTA at 1000 °C for 30 s for good Ohmic contact with metal electrodes. Self-assembled molecular monolayers were then grafted on these samples.

Monolayer Formation

Phosphorus trichloride (99%, PCl_3, 1 mL) was purchased from Innochem Co. Ltd. Triethylamine [99.5%, $N(CH_2CH_3)_3$, 2.5 mL] and benzene (99.7%, C_6H_6, 10 mL) were ordered from Aladdin, Shanghai. The mixed chemicals were transferred into a reaction flask and degassed using the mechanical pump for at least three cycles. Double-side polished intrinsic SOI (100) wafers with a 10 µm thick device layer (resistivity > 10 kΩ·cm) and a buried 1 µm thick silicon dioxide layer were diced into 1 × 1 cm^2 pieces and cleaned sequentially using acetone, ethanol, and DI water, followed by sonication for 10 min to remove particles generated during dicing. In the next step, the wafers were placed in piranha solution [98% H_2SO_4/30% H_2O_2 = 3:1 (v/v)] at 120 °C for 45 min to remove the organic residues on the silicon surfaces. Thereafter, the pieces were dipped in 2.5% aqueous HF to remove the native silicon oxide layer and yield an OH-terminated surface. After rinsing in DI water (resistivity > 18.2 MΩ·cm) and drying in a N_2 stream, the cleaned silicon pieces were transported into the reaction flask in a glovebox filled with argon gas. The P-containing monolayer in the form of a P–O–Si chemical bond was grafted on the SOI surface by heating the reaction flask up to 70 °C in an oil bath overnight under a continuous argon

inflow. After the reaction, the pieces were rinsed with an excessive amount of CMOS grade acetone, ethanol, and DI water, followed by sonication for 10 min to remove any physisorbed material.

FLA Process

The whole FLA chamber mainly consists of a xenon lamp for annealing at the top and a halogen lamp for preheating the samples at the bottom. To ensure that the temperature is uniform on the wafer, a special reflector was designed at the top of the chamber. Nitrogen gas was introduced into the water-cooled annealing chamber. Preheating temperatures of 400–500 K were adopted to reduce the mechanical stress with the energy duration of 3 or 20 ms. The energy density of annealing can be adjusted by changing the power of the xenon lamp.

MBE Growth Technique

The solid-source MBE was utilized to grow 25 nm crystalline silicon in an ultrahigh-vacuum environment. The samples were first baked in the cavity at 120 °C for 5 h to remove the moisture and degassed at 400 °C for 5 min. Gradually, it ramps up to 600 °C to break the Si–H bond, and the Si atom was blended into the substrate lattice by interatomic migration. To minimize the internal diffusion of dopants, the growth was performed at 350 °C.

SIMS Measurements

The samples were dipped in HF to remove the oxidation layers. The phosphorus depth profiles were conducted at EAG Materials Technology Co. Ltd. in Shanghai. A focused Cs^+ primary ion beam with 2 keV and 400 nA was used to motivate the high yields of secondary ions of phosphorus in a CAMECA system. The error of data was less than 10% as determined from multiple measurements in different regions of the same sample.

Magnetoresistance Measurements

The magnetoresistance measurements were performed in a physical property measurement system (PPMS) with liquid helium cooling. The device was mounted on a fixed stage perpendicular to the magnetic field. The maximum field can reach 10 T in liquid He (T = 2 K).

Photoresponse Characterizations

The Keithley 2400 SourceMeter was used to measure the I–V characteristics in the dark and under illumination. The spectral responsivity (230–500 nm) was measured by illuminating the device with a 450 W xenon lamp with a line spectrum through a color filter, and the photocurrent signals were recorded using a Keithley 2400 SourceMeter. Currents were collected at different wavelengths, and the light intensity was calibrated with a commercial Si photodiode (1.2 mm × 1.2 mm square) placed at the same distance and location on the probe station as the samples.

Acknowledgments

This work was financially supported by the National Natural Science Foundation of China (NSFC no. 92065103) and the special-key project of Innovation Program of Shanghai Municipal Education Commission (No. 2019-07-00-02-E00075). XPS, atomic force microscopy, and Hall effect measurements were carried out at the Instrumental Analysis Centre, Shanghai Jiao Tong University. The lithography and etching for device fabrication were performed at the Center for Advanced Electronic Materials and Devices, Shanghai Jiao Tong University.

References

1. Gossmann, H.-J.; Schubert, E. F. Delta Doping in Silicon. Crit. Rev. Solid State Mater. Sci. 1993, 18, 1–67, DOI: 10.1080/10408439308243415

2. Popović, R. S.; Solt, K.; Falk, U.; Stoessel, Z. A Silicon Ultraviolet Detector. Sens. Actuators, A 1990, 22, 553– 558, DOI: 10.1016/0924-4247(89)80034-2

3. Wood, A. C. G.; O'Neill, A. G. Channel Profile Engineering of MOSFETs Using Delta Doping. MRS Online Proc. Libr. 1991, 220, 465, DOI: 10.1557/PROC-220-465

4. Yokogawa, T.; Takahashi, K.; Kusumoto, O.; Uchida, M.; Yamashita, K.; Kitabatake, M. 4H-SiC Delta-Doped Accumulation-Channel MOSFET. Mater. Sci. Forum 2002, 389–393, 1077– 1080, DOI: 10.4028/www.scientific.net/msf.389-393.1077

5. Schubert, E. F.; Cunningham, J. E.; Tsang, W. T.; Timp, G. L. Selectively δ-Doped AlxGa1–xAs/GaAs Heterostructures with High Two-Dimensional Electron-Gas Concentrations 2DEG n≥1.5×1012cm–2 for Field-Effect Transistors. Appl. Phys. Lett. 1987, 51, 1170– 1172, DOI: 10.1063/1.98722

6. Torregrosa, F.; Laviron, C.; Faik, H.; Barakel, D.; Milesi, F.; Beccaccia, S. Realization of Ultra Shallow Junctions by PIII: Application to Solar Cells. Surf. Coat. Technol. 2004, 186, 93– 98, DOI: 10.1016/j.surfcoat.2004.04.046

7. Yakimov, A.; Kirienko, V.; Timofeev, V.; Bloshkin, A.; Dvurechenskii, A. Influence of Delta-Doping on The Hole Capture Probability in Ge/Si Quantum Dot Mid-Infrared Photodetectors. Nanoscale Res. Lett. 2014, 9, 504, DOI: 10.1186/1556-276x-9-504

8. Holz, P. C.; Dechant, A.; Lutz, E. Infinite Density for Cold Atoms in Shallow Optical Lattices. Europhys. Lett. 2015, 109, 23001, DOI: 10.1209/0295-5075/109/23001

9. Normann, H. B.; Vines, L.; Privitera, V.; Skorupa, W.; Schumann, T.; Svensson, B. G.; Monakhov, E. V. Phosphorus in-Diffusion From a Surface Source by Millisecond Flash Lamp Annealing for Shallow Emitter Solar Cells. Appl. Phys. Lett. 2013, 102, 132108, DOI: 10.1063/1.4800781

10. Prucnal, S.; Rebohle, L.; Skorupa, W. Doping by Flash Lamp Annealing. Mater. Sci. Semicond. Process. 2017, 62, 115– 127, DOI: 10.1016/j.mssp.2016.10.040

11. Gao, X.; Guan, B.; Mesli, A.; Chen, K.; Dan, Y. Deep Level Transient Spectroscopic Investigation of Phosphorus-Doped Silicon by Self-Assembled Molecular Monolayers. Nat. Commun. 2018, 9, 118, DOI: 10.1038/s41467-017-02564-3

12. Li, K.; Zhang, J.-Y.; Chang, S.; Wei, H.; Zhang, J.-J.; Dan, Y. Full Activation of Dopants by Carbon-Free Self-Assembled Molecular Monolayer Doping. ACS Appl. Electron. Mater. 2021, 3, 3346– 3351, DOI: 10.1021/acsaelm.1c00276

13. Gouzman, I.; Dubey, M.; Carolus, M. D.; Schwartz, J.; Bernasek, S. L. Monolayer vs. Multilayer Self-Assembled Alkylphosphonate Films: X-Ray Photoelectron Spectroscopy Studies. Surf. Sci. 2006, 600, 773–781, DOI: 10.1016/j.susc.2005.11.030

14. Juang, A.; Scherman, O. A.; Grubbs, R. H.; Lewis, N. S. Formation of Covalently Attached Polymer Overlayers on Si(111) Surfaces Using Ring-Opening Metathesis Polymerization Methods. Langmuir 2001, 17, 1321– 1323, DOI: 10.1021/la0012945

15. Smith, M. P.; McMahon, R. A.; Voelskow, M.; Skorupa, W.; Stoemenos, J.; Ferro, G. Process Control and Melt Depth Homogenization For SiC-on-Si Structures During Flash Lamp Annealing by Carbon Implantation. J. Appl. Phys. 2006, 100, 094909, DOI: 10.1063/1.2359684

16. Polley, C. M.; Clarke, W. R.; Miwa, J. A.; Scappucci, G.; Wells, J. W.; Jaeger, D. L.; Bischof, M. R.; Reidy, R. F.; Gorman, B. P.; Simmons, M. Exploring The Limits of N-Type Ultra-Shallow Junction Formation. ACS Nano 2013, 7, 5499– 5505, DOI: 10.1021/nn4016407

17. Thompson, P. E.; Hobart, K. D.; Twigg, M. E.; Rommel, S. L.; Jin, N.; Berger, P. R.; Lake, R.; Seabaugh, A. C.; Chi, P. H.; Simons, D. S. Epitaxial Si-Based Tunnel Diodes. Thin Solid Films 2000, 380, 145– 150, DOI: 10.1016/s0040-6090(00)01490-5

18. Boeisenko, V. E.; Yudin, S. G. Steady-State Solubility of Substitutional Impurities in Silicon. Phys. Status Solidi A 1987, 101, 123– 127, DOI: 10.1002/pssa.2211010113

19. Trumbore, F. A. Solid Solubilities of Impurity Elements in Germanium and Silicon. Bell Syst. Tech. J. 1960, 39, 205– 233, DOI: 10.1002/j.1538-7305.1960.tb03928.x

20. Altermatt, P. P.; Schenk, A.; Schmithüsen, B.; Heiser, G. A Simulation Model for The Density of States and for Incomplete Ionization in Crystalline Silicon. I. Establishing the Model in Si:P. J. Appl. Phys. 2006, 100, 113715, DOI: 10.1063/1.2386935

21. Ruess, F. J.; Oberbeck, L.; Simmons, M. Y.; Goh, K. E. J.; Hamilton, A. R.; Hallam, T.; Schofield, S. R.; Curson, N. J.; Clark, R. G. Toward Atomic-Scale Device Fabrication in Silicon Using Scanning Probe Microscopy. Nano Lett. 2004, 4, 1969– 1973, DOI: 10.1021/nl048808v

22. Beenakker, C. W. J.; van Houten, H. Quantum Transport in Semiconductor Nanostructures. Solid State Phys. 1991, 44, 1– 228, DOI: 10.1016/s0081-1947(08)60091-0

23. Bishop, D. J.; Tsui, D. C.; Dynes, R. C. In Weak Localization in Silicon MOSFETs: Isotropic and Anisotropic Two-Dimensional Electron Gases. Springer Ser. Solid-State Sci. 1985, 61, 31– 37, DOI: 10.1007/978-3-642-82516-3_4

24. Bergmann, G. Weak Localization in Thin Films: A Time-of-Flight Experiment With Conduction Electrons. Phys. Rep. 1984, 107, 1– 58, DOI: 10.1016/0370-1573(84)90103-0

25. Chakravarty, S.; Schmid, A. Weak Localization: The Quasiclassical Theory of Electrons in A Random Potential. Phys. Rep. 1986, 140, 193– 236, DOI: 10.1016/0370-1573(86)90027-x

26. McPhail, S.; Yasin, C. E.; Hamilton, A. R.; Simmons, M. Y.; Linfield, E. H.; Pepper, M.; Ritchie, D. A. Weak Localization in High-Quality Two-Dimensional Systems. Phys. Rev. B: Condens. Matter Mater. Phys. 2004, 70, 245311, DOI: 10.1103/physrevb.70.245311

27. Simmons, M. Y.; Hamilton, A. R.; Pepper, M.; Linfield, E. H.; Rose, P. D.; Ritchie, D. A. Weak Localization, Hole-Hole Interactions, and The “Metal”-Insulator Transition in Two Dimensions. Phys. Rev. Lett. 2000, 84, 2489– 2492, DOI: 10.1103/physrevlett.84.2489

28. Hikami, S.; Larkin, A. I.; Nagaoka, Y. Spin-Orbit Interaction and Magnetoresistance in The Two Dimension Random System. Prog. Theor. Phys. 1980, 63, 707– 710, DOI: 10.1143/ptp.63.707

29. Butcher, P. N.; March, N. H.; Tosi, M. P. Theory of Electron Transport in Low-Dimensional Semiconductor Structures. In Physics of Low-Dimensional Semiconductor Structures; Springer US: Boston, MA, 1993; pp 95– 176

30. Sarachik, M. P.; Simonian, D.; Kravchenko, S. V.; Bogdanovich, S.; Dobrosavljevic, V.; Kotliar, G. Metal-Insulator Transition in Si:X (X=P, B): Anomalous Response to A Magnetic Field. Phys. Rev. B: Condens. Matter Mater. Phys. 1998, 58, 6692– 6695, DOI: 10.1103/physrevb.58.6692

31. Goh, K. E. J.; Oberbeck, L.; Simmons, M. Y.; Hamilton, A. R.; Butcher, M. J. Influence of Doping Density on Electronic Transport in Degenerate Si:P δ-Doped Layers. Phys. Rev. B: Condens. Matter Mater. Phys. 2006, 73, 035401, DOI: 10.1103/physrevb.73.035401

32. Greer, F.; Hamden, E.; Jacquot, B. C.; Hoenk, M. E.; Jones, T. J.; Dickie, M. R.; Monacos, S. P.; Nikzad, S. Atomically Precise Surface Engineering of Silicon CCDs for Enhanced UV Quantum Efficiency. J. Vac. Sci. Technol., A 2013, 31, 01A103, DOI: 10.1116/1.

33. Mu, J.; Lin, P.-T.; Zhang, L.; Michel, J.; Kimerling, L. C.; Jaworski, F.; Agarwal, A. Design and Fabrication of a High Transmissivity Metal-Dielectric Ultraviolet Band-Pass Filter. Appl. Phys. Lett. 2013, 102, 213105, DOI: 10.1063/1.4807925